Features and Characteristics of the new NASA MicroPuLse NETwork (MPLNET) automatic rain detection algorithm

S. Lolli[1], E. J. Welton[2], J. R. Lewis[3], J. R. Campbell[4] and G. Vivone[1]
[1]CNR-IMAA, Contrada S. Loja snc, Tito Scalo (PZ), 85050, Italy
[2]NASA GSFC, Code 612, Greenbelt, MD 20771, USA
[3]UMBC-JCET, 1000 Hilltop Circle, Baltimore, MD 21250, USA
[4]Naval Research Laboratory, 7 Grace Hopper Ave, Monterey, CA 93943

Email: simone.lolli@imaa.cnr.it (Corresponding author)

Abstract. The water cycle strongly influences life on Earth. In particular, the precipitation modifies the atmospheric column thermodynamics through the process of evaporation and serves as a proxy for latent heat modulation. For this reason, a correct precipitation parameterization (especially low-intensity precipitation) at global scale, bedsides improving our understanding of the hydrological cycle, it is crucial to reduce the associated uncertainty of the global climate models to correctly forecast future scenarios, i.e. to apply fast mitigation strategies. In this study we developed an algorithm to automatically detect precipitation from lidar measurements obtained by the National and Aeronautics Space Administration (NASA) Micropulse lidar network (MPLNET) permanent observational site in Goddard. The algorithm, once full operational, will deliver in Near Real Time (latency 1.5h) a new rain mask product that will be publicly available on MPLNET website as part of the new Version 3 Level 1.5 data. The methodology, based on an image processing technique, can detect only light precipitation events (defined by intensity and duration) as the morphological filters used through the detection process are applied on the lidar volume depolarization ratio range corrected composite images, i.e. heavy rain events are unusable as the lidar signal is completely extinguished after few meters in the precipitation or no signal detected because of the water accumulated on the receiver optics.
Keyword: idar; aerosol; aerosol-cloud interactions; MPLNET; image processing; precipitation; network; infrastructure; virga.

Introduction

Human life is strongly dependent on the water cycle. In particular, precipitation is a key-player in paring the Earth-atmosphere water and energy cycle by modulating the atmospheric column latent heat and affecting cloudiness and cloud lifetime. For this reason, long-term precipitation data observations are needed to analyze precipitation trend and variability, especially at global scale [1]. In the last two decades, thanks to the internet, ground-based network of instruments started to develop and measure important climate-related variables [2], as the columnar and atmospheric profile of aerosol optical and micro-physical properties through passive and active optical sensors, i.e. sun-photometers and lidars. The latter are active optical remote sensing instruments that uses a laser source [3] to sound the atmosphere. Elastic [4], multi-wavelength [5] and Doppler [6] lidar observations are mainly used to study and assess aerosol [7,8,9] and clouds [10,11,12] geometrical and optical properties. On the contrary, lidar measurements containing raining events are usually unjustifiably disregarded, even if light rain events are clearly detectable on lidar data, as shown in Figure 1

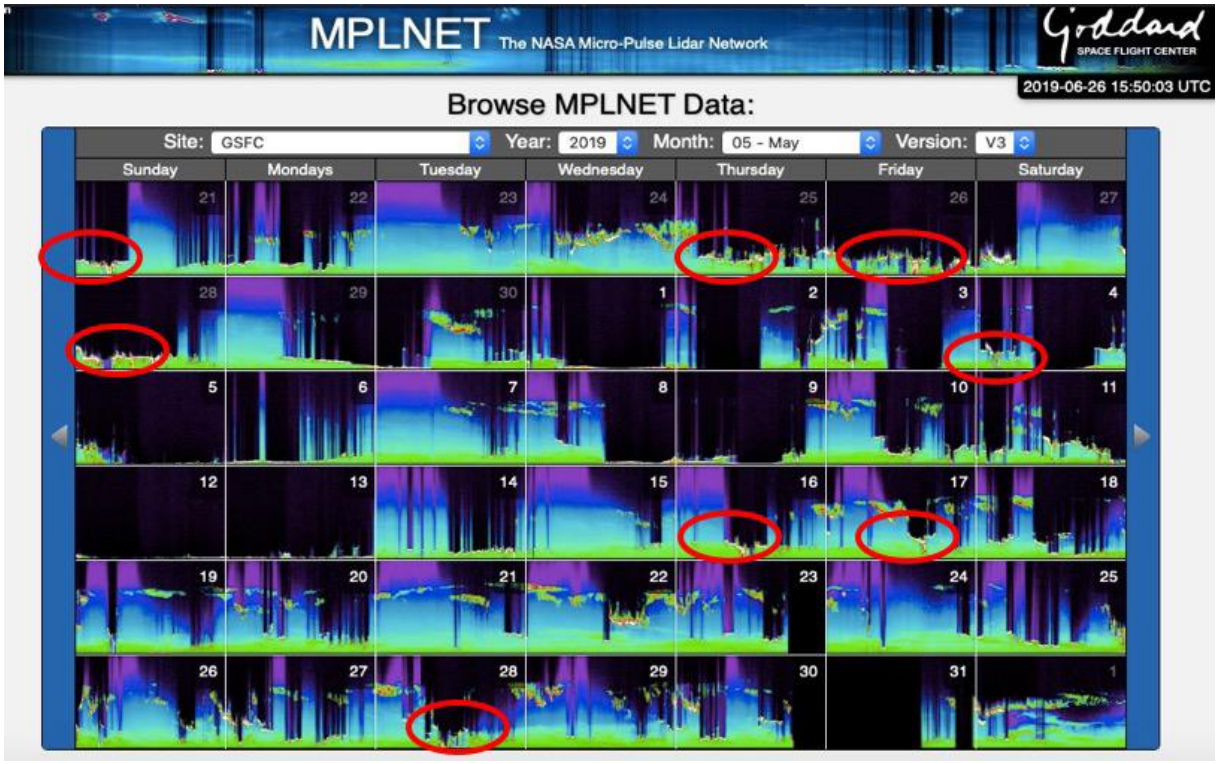

Figure 1: May 2019 thumbnails showing the daily MPLNET V3 NRB variable (L15 MPLNET NRB product). Red circles highlight precipitation events

where several precipitation events are highlighted in red during May 2019 at NASA Goddard Flight Space Center (GSFC). Figure 2 shows the composite plot of the Normalized Relative Backscatter (NRB)(Fig. *2a*) and the Volume Depolarization Ratio (VDR) (Fig. *2b*) range corrected signals on 22 April 2016 at NASA GSFC site.

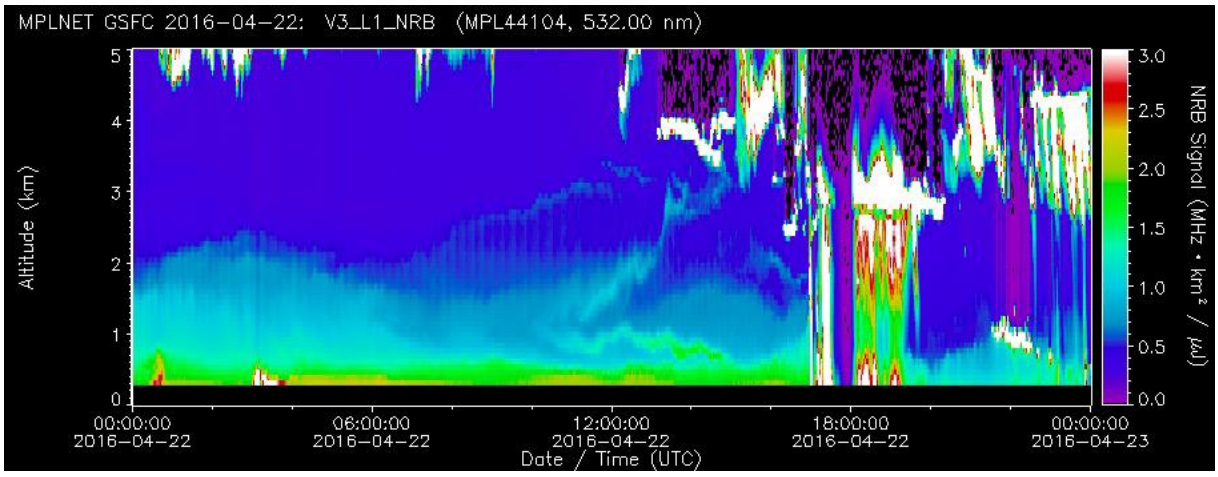

(a) NRB variable composite image on 22 April 2016 observed at NASA Goddard Space Flight Center permanent MPLNET observational site.

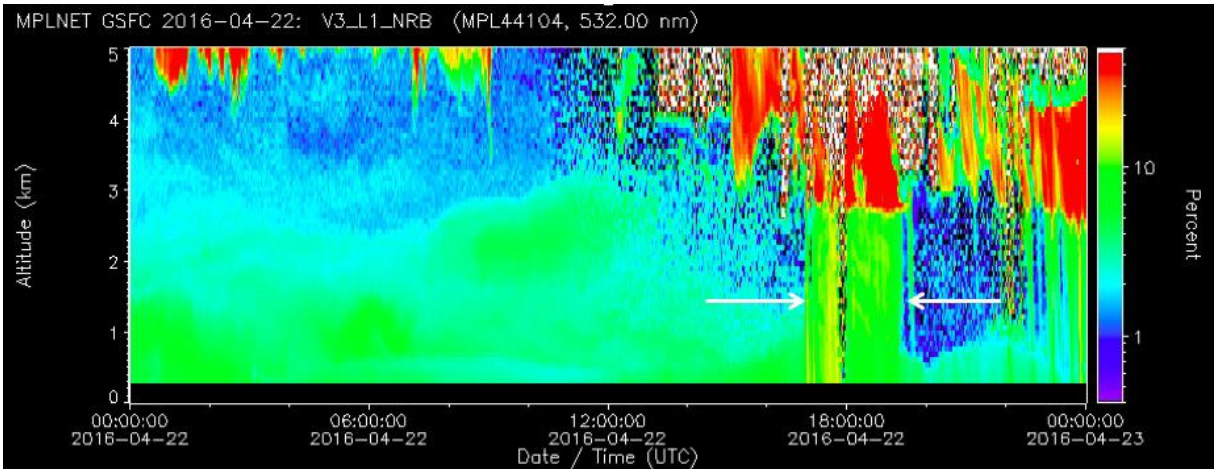

(b) VDR variable composite image on 22 April 2016 observed at NASA Goddard Space Flight Center permanent MPLNET observational site. The horizontal white arrows show the beginning and the end of the precipitation event, while clouds are represented in red

Figure 2: Precipitation event detected on 22 April 2016. With respect to *(a)* NRB, precipitation on *(b)* VDR has more defined and sharp contours (contrast is enhanced). For this reason, the detection is easier on (b)

A precipitation event is displayed as a vertical structure right after 1800UTC. Some recent studies put in evidence that a correct precipitation parameterization[13] will drastically improve global climate models to forecast future scenarios on climate. Further, precipitation studies are crucial to assess aerosol indirect and semi-direct effects because aerosols aspect both cloud formation and precipitation, that in turn removes aerosols from the atmosphere by scavenging effect. Isolated case studies using lidar data (together with ancillary instrumentation) to quantitatively assess the atmospheric profile of precipitation microphysical and optical characteristics are shown in [14,15,16,17]. Nevertheless, the previous cited methods, due to their intrinsic complexity, are not suitable to be operationally implemented in a network. For this reason, we developed and tested an operational automatic algorithm to be implemented in the NASA MPLNET [18] Version 3 (V3) network with the main scope of providing a rain mask product that will be an additional feature of the Level 1.5 (L15) already available cloud algorithm product. The publicly available L15 rain mask might be used as a starting point to further investigate scientifically interesting cases to assess precipitation optical and microphysical properties, or simply to better characterize precipitation patterns and its variability at global scale from the MPLNET (or other networks) database. The developed algorithm, based on image processing techniques, is based on the application of morphological filters to the MPLNET Level 1.5 (L15) cross-polar channel Normalized Range

Methodology

The proposed algorithm, as shown in the flowchart below (Figure 3), is based on the image processing techniques. As first step, the algorithm acquires the Volume Depolarization Ratio (VDR) composite image (L15 MPLNET product). Then, the acquired image is paired with the L15 MPLNET cloud mask product, because the precipitation detection is uniquely carried out under a cloud base, given by the cloud mask [19] (natural rain doesn't exist on clear sky conditions). For this reason, the algorithm will label a bin as "rain" only if it is topped by a cloud. As shown in in the flowchart in Figure 3, the a-priori probability rain detection is provided just exploiting the different threshold of the rain backscattered energy with respect to the aerosols and molecules. Assuming Laplace distributed data the a-priori probability rain detection is maximized for each singular bin to produce a preliminary rain mask. During

post-processing phase, the morphological filters are applied to cancel the image noise due to the signal extinction above the clouds and to remove any not-rectangular shaped detection to produce the final rain mask. The algorithm is currently set-up to detect rain events for cloud bases above 400m from and for precipitations that lasts 5 minutes or more.

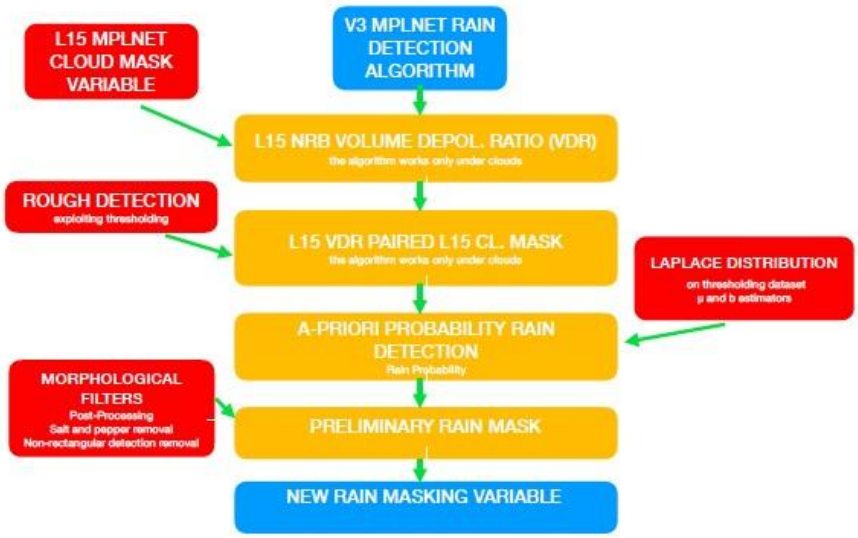

Figure 3: Flowchart of V3 MPLNET rain detection algorithm. A detailed description of all the steps can be found in the corp of the text

Results and discussions

Rain events detected by the developed algorithm are intercompared by rain intensity measurements obtained from a co-located ground based disdrometer at NASA GSFC, which is an in-situ measurement device designed to measure the drop size distribution (DSD;[20]), represented as the number of drops per unit of volume and per unit of raindrop diameter. Disdrometers can be based on different measurement principles (high-speed cameras, Doppler effect, laser-optical, impact, etc.). The second generation Parsivel (Parsivel2) laser-optical disdrometer manufactured by OTT[21] is used in this work . Parsivel systems were originally developed by PM Tech Inc., Germany. The instrument has a laser diode (emitting wavelength of 780 nm) generating a horizontal at beam with a measurement area of 54 cm2. Disdrometer functioning principle is also based on laser technology. When a hydro-meteor passes through the laser beam, it produces attenuation proportional to its size. A relationship between the laser beam occlusion by the falling particle is applied to estimate the particle size. Parsivel instruments can measure particle diameters up to about 25 mm classifying them in 32 size classes of different width. The instrument also estimates the hydro-meter fall velocity by measuring the time necessary for the particle to pass through the laser beam, and thus it stores particles in 32x32 matrices. The disdrometers high temporal resolution (60s here) permits study in great detail of physical precipitation variability.

As previously described, the rain detection algorithm at first pairs the Volume Depolarization Ratio (VDR) composite image with the L15 cloud masking variable. Then, a first guess of rain probability is produced only for the VDR signal above a certain threshold and below a cloud base, i.e. on deep blue regions topped by cyan cloud regions of upper middle plots of Figure 4. The cloud base is never below 400m and the precipitation intensity is very low, i.e. 0.25 mm hr-1 on daily average. Those intensities cannot attenuate completely the lidar signal. Two virga streaks are detected by the algorithm in the second half of the day. The retrieved disdrometer rain rate (Fig. 4; bottom), shows very low values, with

a maximum of 0.76 mm hr-1 at 1701 UTC. The agreement is excellent, however the rain intensity drops so much after 1815UTC that the disdrometer is unable to detect precipitation, but it is clearly visible in the rain mask. Precipitation events from lidar data are then necessary to fill a gap in detecting very low precipitation intensity events (less than 0.05 mm hr-1) that are crucial to study the aerosol effects and interactions on clouds and precipitations.

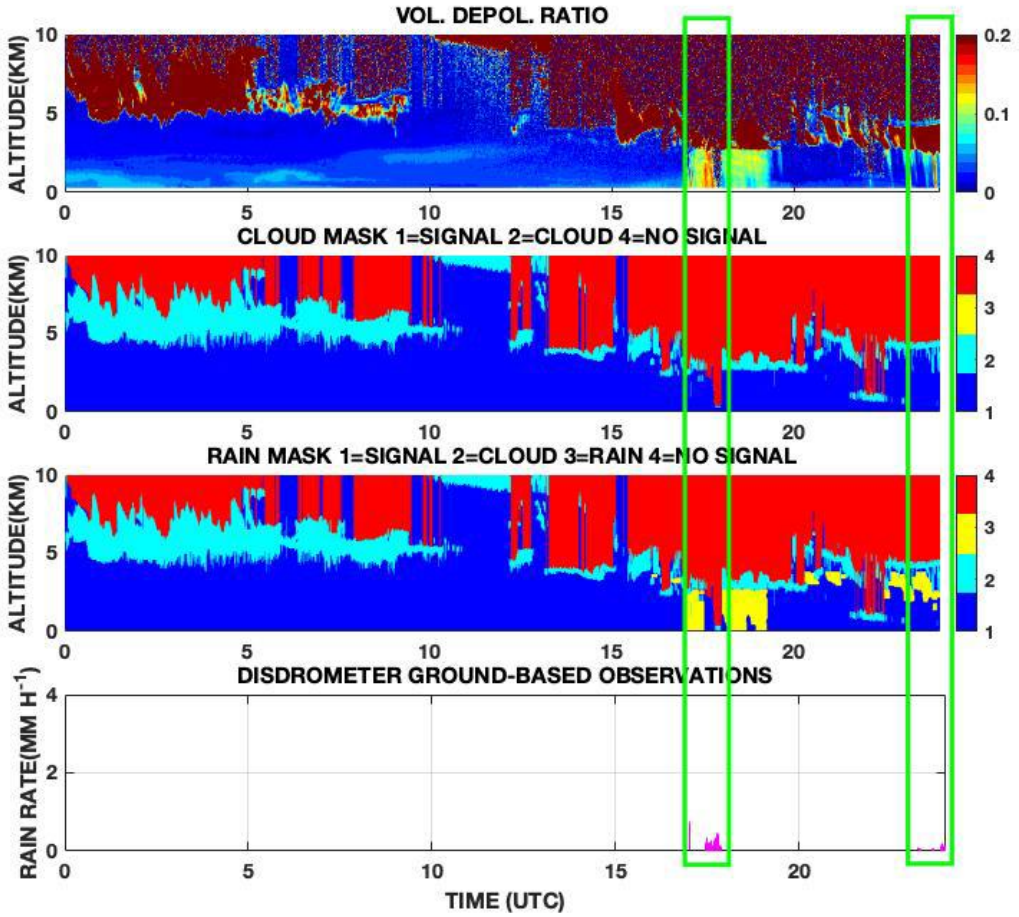

Figure 4: Rain mask variable from rain detection algorithm on 22 April 2016 from MPLNET observation at NASA GSFC (Lat:38.99N, Lon:76.38W, Alt:50m a.s.l.). The different steps to obtain the rain mask are shown in the flowchart in Fig. 3 :Upper: Volume depolarization ratio variable obtained from MPLNET NRB L15 signal product. Middle 1: Cloud mask variable from MPLNET L15 CLD product. The algorithm retrieves precipitation only on blue regions topped by clouds (cyan bins). Middle 2: New rain mask product (rain plotted in yellow) Lower:Co-located precipitation intensity measured by disdrometer. The green rectangular shapes help in visualizing the detected rain events

The rain detection algorithm has been validated vs. observations obtained from the ground based co-located disdrometer over 7 days (not shown in here). The intercomparison results show a 100% success detection rate of the algorithm. A detection is considered successful if the precipitation detected by the algorithm and by the disdrometer are superimposing at least for 1 minute (or more). Lidar data are not suitable to detect strong precipitation events, while can detect virga streaks (a precipitation type that doesn't reach the ground because of evaporation) and very low intensity rain (less than 0.05 mm hr-1).

Conclusions

The developed algorithm is proven to be effective in detecting rain episodes from lidar observations. Nevertheless, due to the nature of lidar instrument, the technique is limited in case of strong precipitation events. The implementation of the algorithm operationally in the NASA MPLNET lidar netowrk will fill a gap left by TRMM and GPM missions in detecting low intensity precipitations, crucial to improve global climate model forecasts and for aerosol-cloud and in turn precipitation interactions. Being the methodology used in developing the algorithm based on image-processing techniques, in future the algorithm will be tested on ceilometer data, where also the precipitation produces a higher-contrasted feature in the range corrected backscattered signal**.**

References

[1] Koster, R. D., Suarez, M. J., and Heiser, M., Variance and predictability of precipitation at seasonal-to- interannual timescales," *Journal of Hydrometeorology* 1(1), 26{46 (2000).
[2] Lolli, S. and Di Girolamo, P., Principal component analysis approach to evaluate instrument performances in developing a cost-effective reliable instrument network for atmospheric measurements," *J. Atmos. Ocean. Technol.* 32(9), 1642{1649 (2015).
[3] Ciofini, M., Lapucci, A., and Lolli, S., Diffractive optical components for high power laser beam sampling," *J. Opt. A: Pure Appl. Opt.* 5(3), 186 (2003).
[4] Lolli, S., Sauvage, L., Loaec, S., and Lardier, M., Ez lidar: A new compact autonomous eye-safe scanning aerosol lidar for extinction measurements and pbl height detection. validation of the performances against other instruments and intercomparison campaigns," *Optica pura y aplicada* 44(1), 33{41 (2011).
[5] Lolli, S., Madonna, F., Rosoldi, M., Campbell, J. R., Welton, E. J., Lewis, J. R., Gu, Y., and Pappalardo, G., Impact of varying lidar measurement and data processing techniques in evaluating cirrus cloud and aerosol direct radiative effects," *Atmospheric Measurement Techniques* 11(3), 1639 (2018).
[6] Lolli, S., Delaval, A., Loth, C., Garnier, A., and Flamant, P., \0.355-micrometer direct detection wind lidar under testing during a field campaign in consideration of Esa's adm-aeolus mission," *Atmos. Meas. Tech.* 6, 3349{3358 (2013).
[7] Reid, J. S., Lagrosas, N. D., Jonsson, H. H., Reid, E. A., Atwood, S. A., Boyd, T. J., Ghate, V. P., Xian, P., Posselt, D. J., Simpas, J. B., et al., Aerosol meteorology of maritime continent for the 2012 7seas southwest monsoon intensive study part 2: Philippine receptor observations of _ne-scale aerosol behavior," *Atmospheric Chemistry and Physics* 16(22), 14057{14078 (2016).
[8] Lolli, S., Alparone, L., Garzelli, A., and Vivone, G., \Haze correction for contrast-based multispectral pansharpening," IEEE Geosci. Remote Sens. Lett. 14(12), 2255{2259 (2017).
[9] Bilal, M., Nazeer, M., Nichol, J. E., Bleiweiss, M. P., Qiu, Z., Jkel, E., Campbell, J. R., Atique, L., Huang, X., and Lolli, S., A simplified and robust surface reflectance estimation method (srem) for use over diverse land surfaces using multi-sensor data," Remote Sensing 11(11) (2019).
[10] Campbell, J. R., Lolli, S., Lewis, J. R., Gu, Y., and Welton, E. J., Daytime cirrus cloud top-of-the atmosphere radiative forcing properties at a midlatitude site and their global consequences," *J. Appl. Meteorol. Climatol.* 55(8), 1667{1679 (2016).
[11] Lolli, S., Campbell, J. R., Lewis, J. R., Gu, Y., Marquis, J. W., Chew, B. N., Liew, S.-C., Salinas, S. V. and Welton, E. J., Daytime top-of-the-atmosphere cirrus cloud radiative forcing properties at Singapore, *J. Appl. Meteorol. Climatol.* 56(5), 1249{1257 (2017).
[12] Campbell, J., Peterson, D., Marquis, J., Fochesatto, G., Vaughan, M. A., Stewart, S. A., Tackett, J., Lolli, S., Lewis, J., Oyola, M., and Welton, E., Unusually deep wintertime cirrus clouds observed over the Alaskan subarctic," *Bulletin of the American Meteorological Society* 99(1), 27{32 (2018).

[13] Campbell, J. R., Ge, C., Wang, J., Welton, E. J., Bucholtz, A., Hyer, E. J., Reid, E. A., Chew, B. N., Liew, S.-C., Salinas, S. V., et al., \Applying advanced ground-based remote sensing in the southeast Asian maritime continent to characterize regional pro_ciencies in smoke transport modeling," *J. Appl. Meteorol. Climatol*. 55(1), 3{22 (2016).

[14] Westbrook, C., Hogan, R., O'Connor, E., and Illingworth, A., \Estimating drizzle drop size and precipitation rate using two-colour lidar measurements," *Atmospheric Measurement Techniques* 3(3), 671{681 (2010).

[15] Lolli, S., Welton, E. J., and Campbell, J. R., \Evaluating light rain drop size estimates from multiwavelength micropulse lidar network profiling," *J. Atmos. Ocean. Technol*. 30(12), 2798{2807 (2013).

[16] Lolli, S., Di Girolamo, P., Demoz, B., Li, X., and Welton, E., \Rain evaporation rate estimates from dual- wavelength lidar measurements and intercomparison against a model analytical solution," *J. Atmos. Ocean. Technol*. 34(4), 829{839 (2017).

[17] Lolli, S., DAdderio, L. P., Campbell, J. R., Sicard, M., Welton, E. J., Binci, A., Rea, A., Tokay, A., Comeron, A., Barragan, R., Baldasano, J. M., Gonzalez, S., Bech, J., Afflitto, N., Lewis, J. R., and Madonna, F., Vertically resolved precipitation intensity retrieved through a synergy between the ground-based NASA MPLNET lidar network measurements, surface disdrometer datasets and an analytical model solution, *Remote Sens*. 10(7) (2018).

[18] Welton, E. J., Campbell, J. R., Spinhirne, J. D., and Stanley Scott III, V., Global monitoring of clouds and aerosols using a network of micropulse lidar systems," *SPIE Conference Proceedings* 4153 (2001).

[19] Lewis, J. R., Campbell, J. R., Welton, E. J., Stewart, S. A., and Haftings, P. C., \Overview of mplnet version 3 cloud detection," *Journal of Atmospheric and Oceanic Technology* 33(10), 2113-2134 (2016).

[20] D'Adderio, L., Porcù, F., and Tokay, A., Evolution of drop size distribution in natural rain," *Atmospheric Research* 200, 70{76 (2018).

[21] Lffler-Mang, M. and Joss, J., \An optical disdrometer for measuring size and velocity of hydrometeors," Journal of Atmospheric and Oceanic Technology 17(2), 130{139 (2000).